International Journal of Applied Earth Observations and Geoinformation 103 (2021) 102492

Contents lists available at ScienceDirect

International Journal of Applied Earth Observations and Geoinformation

journal homepage: www.elsevier.com/locate/jag

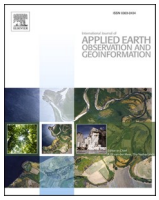

Direction-dominated change vector analysis for forest change detection

Pengfeng Xiao [a,b,*], Guangwei Sheng [a], Xueliang Zhang [a], Hao Liu [a], Rui Guo [a]

[a] Jiangsu Provincial Key Laboratory of Geographic Information Science and Technology, Key Laboratory for Land Satellite Remote Sensing Applications of Ministry of Natural Resources, School of Geography and Ocean Science, Nanjing University, Nanjing, Jiangsu 210023, China
[b] Jiangsu Center for Collaborative Innovation in Geographical Information Resource Development and Application, Nanjing, Jiangsu 210023, China

ARTICLE INFO

Keywords:
Forest
Land cover change
Change detection
Change vector analysis

ABSTRACT

As forest is under increasing pressure, the rapid conversion or degradation of forest has attracted strong concern. Obtaining quantitative information of forest change based on satellite imagery becomes necessary and urgent, especially the detailed "from-to" information. In this study, a semi-automatic method called direction-dominated change vector analysis (DCVA) was proposed to detect "from-to" information of forest change. DCVA is composed of three steps: (1) determining candidate changed pixels, (2) determining direction ranges for different forest change types, and (3) determining final changed pixels for each forest change type. Like the classic change vector analysis (CVA), the magnitude and direction of change vector (CV) are used to detect the changed areas and types in DCVA, respectively. However, CVA is "magnitude-dominated" by setting only one magnitude threshold for different change types, while DCVA is "direction-dominated" by determining change types according to change direction at first, followed by setting different magnitude threshold for each change type. In this case, DCVA holds the advantage of accurately detecting changed areas for different change types by considering the specific characteristics of each change type. Experiments are performed with Sentinel-2A satellite images to demonstrate the advantages of DCVA for forest change detection. The changed areas with four types of forest change were successfully extracted by DCVA. The comparison of both geometric and thematic accuracies between DCVA and CVA further indicates the effectiveness of the proposed method for forest change detection.

1. Introduction

Forest plays a fundamental role in delivering conservation of biodiversity and mitigation of climate change (MacDicken, 2015). As the remaining and accessible forest is under increasing pressure, the rapid conversion or degradation of forest has attracted strong concern (Trumbore et al., 2015). Forest change has been the crucial aspect of change detection using remote sensing technologies (Hussain et al., 2013).

With the improvement of earth observation technology, many change detection methods based on satellite imagery have been developed (Chen et al., 2003, 2012; Hussain et al., 2013; Lu et al., 2004; Singh, 1989; Zhu, 2017). Change detection methods can be categorized into two broad groups: methods based on classification results of input data, such as post-classification comparison (Duveiller et al., 2008), trajectory classification (Cohen et al., 2018), and direct multi-date classification (Lunetta et al., 2006), and methods based on radiometric change between different acquisition dates, such as image algebra methods (Muchoney and Haack, 1994; Oliveira et al., 2019), principal component analysis (PCA) (Byrne et al., 1980; Leichtle et al., 2017; Rokni et al., 2015), Tasseled Cap (TC) transform (Allen et al., 2018; Collins and Woodcock, 1996), change vector analysis (CVA) (Malila, 1980; Sun et al., 2019), and regression analysis (Vogelmann et al., 2016). For end-users, selecting a suitable change detection approach, in practice, often depends on the requirement of application, data availability and quality, time and cost constraints, and analysis skill and experience (Johnson and Kasischke, 1998; Tewkesbury et al., 2015).

Due to forest disturbances, such as deforestation (e.g. clear-cutting and logging) and forest degradation (e.g. fire, disease, and pests) (Cohen et al., 2018; Healey et al., 2018; Trumbore et al., 2015), obtaining detailed change information deserves more attention (MacDicken, 2015). For forest change detection, CVA is an efficient and uncomplicated approach to obtain "from-to" information. Change detection methods such as image differencing can only provide change/no-change (binary) information (Hussain et al., 2013). Methods based on classification can provide "from-to" information, but errors in any of the input maps are directly translated to the change map (Tewkesbury et al., 2015). In CVA, the magnitude of change vector (CV) is used to

* Corresponding author at: School of Geography and Ocean Science, Nanjing University, Nanjing, Jiangsu 210023, China.
E-mail address: xiaopf@nju.edu.cn (P. Xiao).

https://doi.org/10.1016/j.jag.2021.102492
Received 3 February 2021; Received in revised form 13 July 2021; Accepted 8 August 2021
Available online 20 August 2021

discriminate changed pixels whereas the direction of CV depicts change type. Comparing with other change detection methods, CVA can find changed pixels straightforwardly using more (even all) spectral bands and provide detailed "from-to" information avoiding cumulative error in image classification (Chen et al., 2003).

CVA has been widely applied for forest change detection since its first application by Malila (1980) to characterize change magnitude and direction in spectral space. Allen (2000) proposed to form CVs with different combinations of TC indices (brightness, greenness, and wetness) to examine spruce-fir ecosystems. Vegetation indices were also used as features to form CVs (Bayarjargal et al., 2006; Nackaerts et al., 2005). But if CV is only composed of TC indices or vegetation indices, it might lead to a significant loss of information and thus fail to identify some types of change (Bovolo et al., 2012). To make full use of the information presented in remotely sensed images, many modified CVA methods have been proposed for forest change detection. E.g., Zanotta et al. (2014) employed three features in 3-dimensional spherical domain to detect deforestation activities; Chen and Chen (2016) and Sun et al. (2019) utilized both spectral and textural features to extract forest changes. Marinelli et al. (2020) worked in raster domain to compare two lidar datasets to produce a map that identifies the major classes of change occurring in the forest. This is done by analyzing the CVs in terms of magnitude and direction in polar coordinate to discriminate different classes of change.

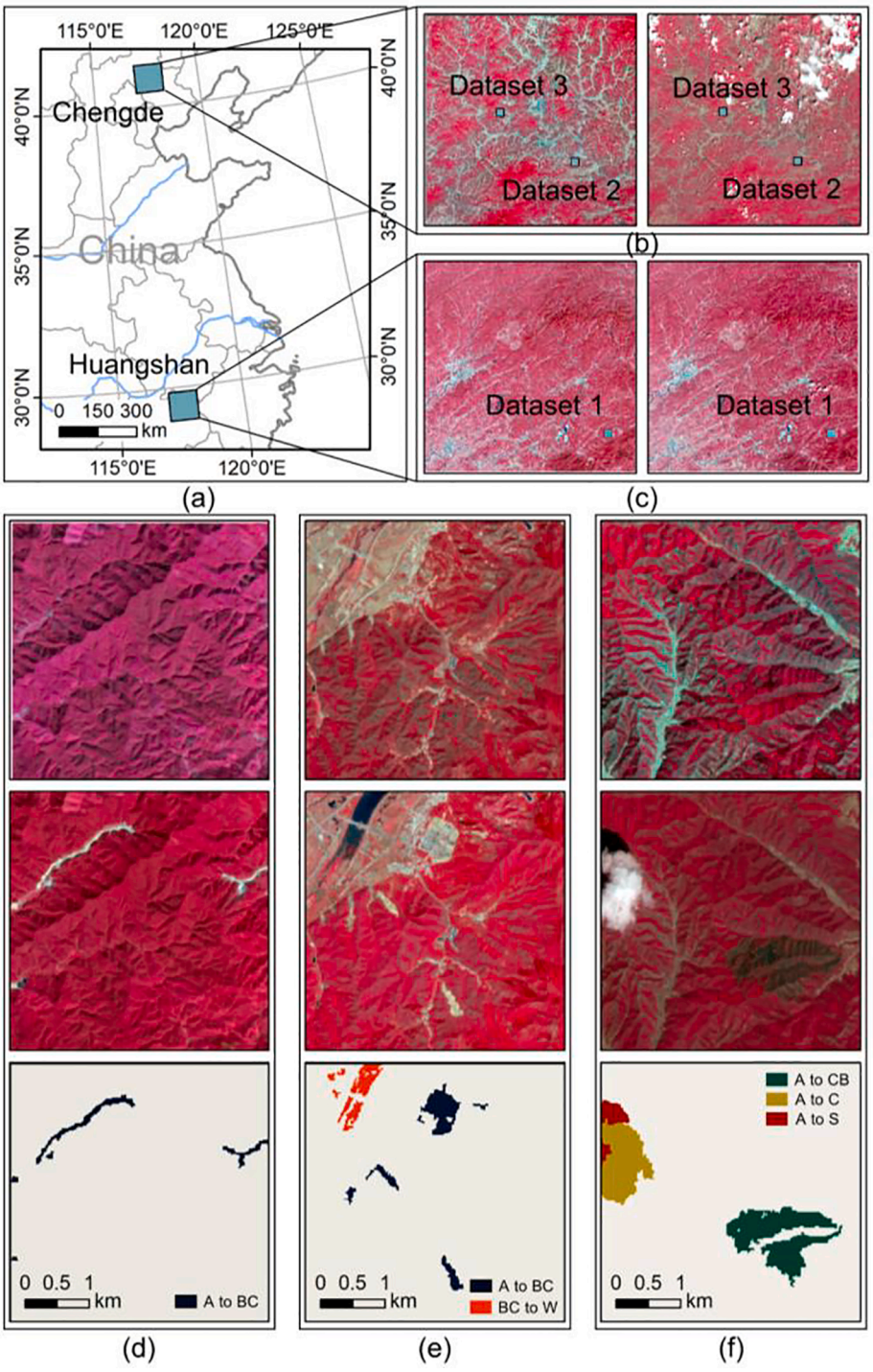

Fig. 1. Study areas and datasets. (a) Location of the study areas in east China; (b) Sentinel-2A images in Chengde acquired on 14 June 2017 (left) and 14 June 2018 (right); (c) Sentinel-2A images in Huangshan acquired on 9 October 2017 (left) and 4 October 2018 (right); (d)–(f) are dataset 1–3, respectively, with image of 2017, image of 2018, and reference of forest changed pixels presented from top to down. The Sentinel-2A images are shown with false color composite (red: near-infrared band; green: red band; blue: green band).

Although the advantages of CVA for forest change detection have been demonstrated in the above-mentioned studies, CVA still has two problems that need to be further explored: for the direction, the pixels with different forest change types correspond to different directions of CVs, and the connections between the direction ranges and the forest change types should be discovered; and for the magnitude, the classic CVA uses only one magnitude threshold to distinguish change and no-change pixels. Even though the multi-threshold CVA determines magnitude thresholds of CVs depend on different land cover categories (Xian et al., 2009), the performance of multiple magnitude thresholds need to be assessed specifically for forest change detection (Bovolo and Bruzzone, 2011; Solano-Correa et al., 2019).

In order to improve the CVA performance of forest change detection, a modified CVA method called direction-dominated change vector analysis (DCVA) is proposed in this study. It is divided into three steps: determining candidate changed pixels, determining direction ranges for different forest change types, and determining final changed pixels for each forest change type.

The main contributions of this study include: identifying the relationship between CVs' direction ranges and forest change types to obtain "from-to" information, applying multiple local magnitude thresholds for different change types to detect forest changed areas, and the advantage of the DCVA method on detecting forest changes is demonstrated by using three datasets of Sentinel-2A images.

The rest of the paper is organized as below. The study areas and datasets are described in Section 2. The proposed DCVA method is delineated in Section 3. The experimental results and discussions are presented in Sections 4 and 5, respectively. Finally, Section 6 draws conclusions of the study.

2. Study areas and datasets

2.1. Study areas

Two forest regions with high coverage rate are selected as the study areas, which are located in Huangshan and Chengde of China (Fig. 1). The study area of Huangshan is in the south of China (40°33′48″–41°32′53″N, 116°59′43″–118°19′1″E). The annual average temperature and precipitation are 16 °C and 1670 mm, respectively. Due to the suitable climate conditions, Huangshan is rich in forest resources, with a forest coverage rate of 83%. The main tree species are fir and pine, which are summarized as arbor in this study. The study area of Chengde is in the north of China (28°50′39″–29°49′15″N 117°0′16″–118°7′53″E). The annual average temperature and precipitation are 9 °C and 512 mm, respectively. Chengde also has abundant forest resources, with a forest coverage rate of 56%. The tree species in Chengde are also dominated by arbor, specifically including mites, aspen, birch, and eucalyptus. Threatened by fast economic development and urban expansion, the forest resources in the two study areas are under increasing pressure. There are numerous forest changes in the study areas caused by human activities.

2.2. Forest change types

Forest changes are generally summarized as forest loss (e.g. deforestation and forest degradation) and forest gain (e.g. afforestation and reforestation). In most cases, forest loss is concentrated and abrupt, and can be clearly documented with a sequence of remote sensing images. Forest gain, in contrast, is a highly variable, dispersed, and protracted process that is challenging to document over short period (Chazdon et al., 2016). Thus, this study only focuses on detecting abrupt changes based on remote sensing images, in which clear-cutting and fire are the main causes.

In terms of deforestation, the forest land will change to cut-over land or bare/construction land. There will be a large amount of vegetation on the surface of cut-over land because of natural regeneration or replanting after harvesting. There will be no vegetation on the surface of bare/construction land because the deforested area is going to be or has been used as an infrastructure.

In terms of forest degradation, only the fire situation appears in the study areas, in which the forest land is changed to burned land. Although a fire will degrade the forest, there will still be vegetation on the surface of burned land because of the natural regeneration.

The change from forest land to cut-over/burned land can be considered as the fluctuation of forest area because the changed areas can be restored to forest after regeneration by natural or artificial means. By contrary, the change from forest to bare/construction land means the absolute reduction of forest area, because it will not be restored to forest after constructing infrastructures.

In addition, since the cloud contamination is unavoidable for optical remote sensing, the change detection result is always influenced by cloud and its shadow. Taking this into consideration, the influence of cloud contamination is also viewed as a change type, e.g. from forest to cloud or to cloud shadow, by which the fake changes caused by cloud can be removed after being detected.

According to the above analysis, the forest change types in the study areas are summarized as four categories: arbor land to bare/construction land (A to BC), arbor land to cut-over/burned land (A to CB), and arbor land to cloud (A to C) or cloud shadow (A to S). The change types are marked as different color in Fig. 1 for the delineated changed pixels. It is noted that there are changes other than forest changes in the study areas, e.g. the change from bare/construction land to water (BC to W) in Fig. 1 (f), which are needed to be discriminated from forest change by the proposed method.

2.3. Datasets

Sentinel-2 images were selected to perform experiments, because they have high-spatial resolution and red-edge bands which are very useful to discriminate vegetation types. Sentinel-2 MultiSpectral Instrument (MSI) covers 13 spectral bands (443–2190 nm), with a swath width of 290 km and a spatial resolution of 10 m (four visible and near-infrared bands), 20 m (six red-edge and shortwave infrared bands) and 60 m (three atmospheric correction bands). The revisit time at equator with only Sentinel-2A satellite is 10 days and with identical twin satellite Sentinel-2B is 5 days from two-satellite constellation.

In order to avoid the influence of vegetation phenology, the selected image pairs should be close to each other in terms of the month in different years. Accordingly, four Sentinel-2A MSI images (Level 1C product) were selected and downloaded from the Sentinels Scientific Data Hub of European Space Agency (ESA). Two of them are over the Huangshan area, acquired on 9 October 2017 and 4 October 2018. The other two images are over the Chengde area, acquired on 14 June 2017 and 14 June 2018. Because the Level 1C product has undergone radiometric and geometric corrections with sub-pixel accuracy, we implemented atmospheric, terrain, and cirrus correction using the Sen2Cor tool (https://step.esa.int/main/snap-plugins/sen2cor/). After that, the nearest neighbor method was used to resample the images into 20-m resolution to reduce the spatial complexity for change detection.

Three regions were selected from the Sentinel-2A images to produce experimental datasets, as shown in Fig. 1. The size of each dataset is 200 × 200 pixels. Dataset 1 is located in Huangshan, whereas dataset 2 and 3 are in Chengde. The forest changed pixels are manually delineated by specialists in remote sensing with the aid of high-spatial resolution images in Google Earth and reviewed by others to catch any obvious errors, which will be used for reference to evaluate the forest change detection methods. Dataset 1, 2, and 3 have 585, 1607, and 4445 changed pixels, respectively. Dataset 1 only has one change type, which is A to BC. For dataset 2, besides A to BC, there is another change type, namely BC to W. Dataset 3 has three change types, including A to CB, A to C, and A to S. The number of changed pixels corresponding to different change types in each dataset is shown in Table 1.

Table 1
Number of changed pixels corresponding to different change types in each dataset.

	A to BC	A to CB	A to C	A to S	BC to W
Dataset 1	585	/	/	/	/
Dataset 2	1000	/	/	/	607
Dataset 3	/	2314	1747	384	/

3. Method

3.1. Framework of direction-dominated change vector analysis

In CVA, the spectral reflectance values are treated as vectors of spectral bands and a CV is calculated by subtracting vectors for a pixel at different dates (Malila, 1980). The magnitude of CV is used to find changed pixels and the direction of CV depicts change type (Hussain et al., 2013).

It is assumed that the remote sensing image acquired at date t_1 is X_1, and the remote sensing image acquired at date t_2 is X_2. Let $X_{t,b}$ ($b = 1, 2, \ldots, B$, where B is the number of participating bands) denote the b-band of image X_t ($t = 1, 2$). The difference image X_D is obtained by subtracting the spectral vectors of each pixel in X_1 and X_2. Accordingly, $X_{D,b}$ denotes the b-band of X_D:

$$X_{D,b} = X_{2,b} - X_{1,b} \tag{1}$$

CV is then calculated based on X_D. Let ρ and θ denote the magnitude and direction of CV, respectively, they can be formulated as:

$$\rho = \sqrt{\sum_{b=1}^{B} X_{D,b}^2} = \sqrt{\sum_{b=1}^{B} \left(X_{2,b} - X_{1,b}\right)^2} \tag{2}$$

$$\theta = \cos^{-1}\frac{1}{\sqrt{B}}\left(\sum\nolimits_{b=1}^{B} X_{D,b} \Big/ \sqrt{\sum\nolimits_{b=1}^{B} X_{D,b}^2}\right), \theta \in [0, \pi] \tag{3}$$

The participated bands for calculating X_D are closely related to the accuracy of change detection results. The Sentinel-2A image has 12 spectral bands, but not all bands are sensitive to forest change. In this study, the selected bands include green, red, red-edge 1, and near-infrared band. The red and near-infrared bands have been widely used to detect changes in forest (Liu et al., 2018). The red-edge band is especially useful for vegetation applications, e.g. discriminating vegetation burn severity (Fernández-Manso et al., 2016) and identifying crop field boundaries (Solano-Correa et al., 2017). In addition, considering that the changes in the study area involve bare/construction land, the green band is incorporated for calculating X_D as it is sensitive to these changes.

The proposed DCVA method is designed to detect the changed pixels and the corresponding change types from X_D. Unlike the classic CVA method, where a global change magnitude threshold is first applied to obtain changed pixels, followed by determining change types, DCVA determines change types at first, and then the threshold of changed pixels for each change type is locally determined. Compared to CVA, the proposed DCVA aims at improving change detection accuracy by applying multiple local change magnitude thresholds for each change type, rather than a single global threshold for all change types. However, directly determining change types from X_D is very difficult because too many unchanged pixels are involved. Hence, the candidate changed pixels are firstly roughly estimated for determining change types. The flow diagram of DCVA is described as Fig. 2, which sequentially includes three steps: determining candidate changed pixels, determining direction ranges for different change types, and determining final changed pixels for each change type.

3.2. Determining candidate changed pixels

The first step is to determine the candidate changed pixels from all pixels by a global threshold T of the change magnitude ρ. Since the candidate changed pixels are only used for determining the change types for the next step, they are allowed to include unchanged pixels or mixed changed pixels. Because the change magnitudes of unchanged pixels tend to be small compared to those of changed pixels, the threshold T of the change magnitude ρ is exploited for distinguishing the candidate changed pixels.

Many thresholding algorithms can be used, such as iterative thresholding, Ostu's method, and expectation maximization (EM) algorithm. The EM algorithm is selected because it is an effective and general approach. It is assumed that both the changed and unchanged pixels obey the Gaussian distribution. Accordingly, all the pixels can be viewed as a Gaussian mixture model (GMM) consisting of two Gaussian models (Bovolo and Bruzzone, 2007). According to the Bayesian decision theory, the threshold T is calculated by estimating the statistical parameters of the two models (Moon, 1996). The pixels with ρ greater than T are determined as the candidate changed pixels.

3.3. Determining direction ranges for different change types

The second step is to determine the change direction ranges for different change types based on the candidate changed pixels. The changed pixels with the same change type are assumed to have similar change direction θ. Accordingly, each change type corresponds to a certain range of change direction θ, as shown in Fig. 3.

Many clustering algorithms can be used, such as k-means, ISODATA, and mean shift. The k-means algorithm is selected because it is simple and effective (Solano-Correa et al., 2019). It is an iterative algorithm that assigns data to exactly one of k clusters defined by centroids, where k should be close to the number of change types in the image, which is acquired based on a priori knowledge of the study area. Certainly, the optimal k can be determined by some automatic methods, such as gap statistic (Tibshirani et al., 2001), elbow method (Thorndike, 1953), and silhouette coefficient (Rousseeuw, 1987). After k-means clustering, the labels of change types are manually assigned to the clusters.

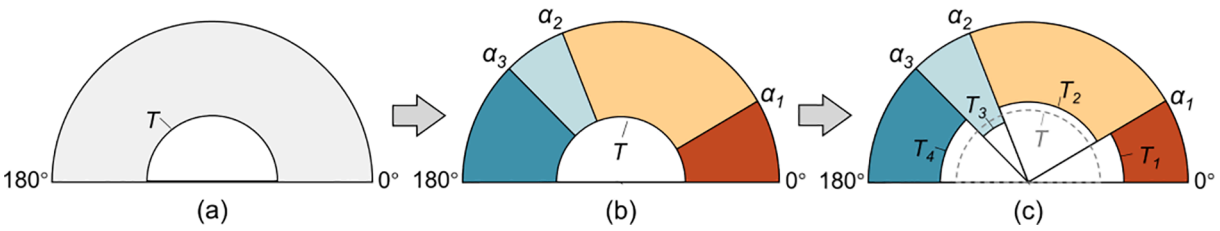

Fig. 2. Flow diagram of the direction-dominated change vector analysis (DCVA) for forest change detection: (a) determining candidate changed pixels (grey area) based on a global magnitude threshold T, (b) determining change types (different colors) based on direction ranges $[0^\circ, \alpha_1)$, $[\alpha_1, \alpha_2)$, $[\alpha_2, \alpha_3)$, and $[\alpha_3, 180^\circ]$, and (c) determining final changed pixels for each change type based on local magnitude threshold T_1, T_2, T_3, and T_4. The feature space is expressed in 2-dimentional space as an example by using the polar coordinate system.

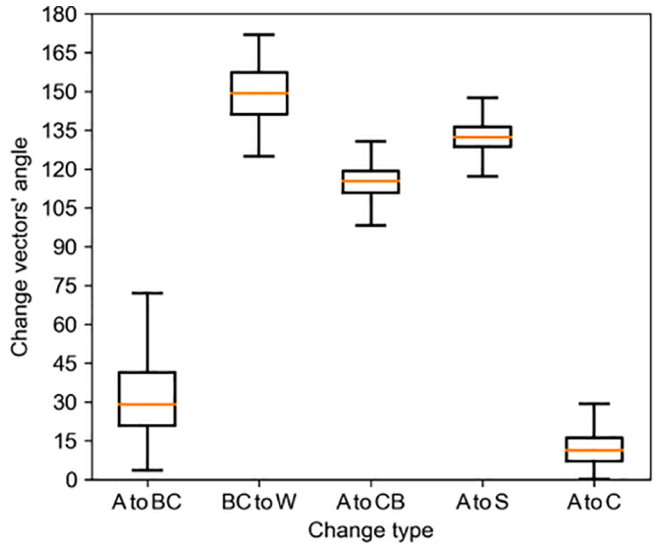

Fig. 3. Boxplot of change vectors' angles corresponding to different change types. The box indicates the first quartile to the third quartile. The horizonal orange line goes through the box at the median. The whiskers go from each quartile to the minimum or maximum.

3.4. Determining final changed pixels for each change type

The third step is to determine the final changed pixels for each change type. It is assumed that the threshold of change magnitude ρ for different forest change types are different with each other. In this case, determining changed pixels with a global threshold would unavoidably bring unchanged pixels or mixed changed pixels. The idea of determining changed pixels for each change type is setting different local thresholds for ρ to overcome the above-mentioned problem and thus to improve the accuracy of detected change pixels.

Specifically, for each change direction range obtained by the second step, the threshold of change magnitude ρ is re-determined based on EM algorithm, thereby obtaining the final changed pixels for the corresponding change type. For each change direction range, two GMM components are used. Generally, the change magnitudes of changed pixels are greater than that of the unchanged pixels, thus the component farther from the minimum represents the changed pixels.

Although the direction ranges for A to BC and A to C are partly overlapped in Fig. 3, so are A to CB, A to S, and BC to W, the thresholds of change magnitude for each direction range are different after implementing the third step, which reduces the miss-classified pixels between different changes. This is just the advantage of the direction-dominated CVA compared to the classic magnitude-dominated CVA. Certainly, there will not be any miss-classified pixels between A to BC and A to C in the study areas, because they occur in different datasets, i.e., A to BC in dataset 1 and 2, but A to C in dataset 3.

3.5. Accuracy assessment

The change detection results are evaluated by comparing with the reference images. Considering that the number of changed pixels is generally much smaller than that of unchanged pixels, the measures of precision (P), recall (R), and F1-score (F) are selected as quantitative indicators for evaluating change detection results. P is used to evaluate the correct rate of the result, i.e. the proportion of true changed pixels in the detected changed pixels. R is used to evaluate the miss rate of the result, i.e. the ratio of the detected true changed pixels to all true changed pixels. F is a combined measure, which is the harmonic mean of P and R. They are calculated as follows:

$$P = \mathrm{TP}/(\mathrm{TP}+\mathrm{FP}) \tag{4}$$

$$R = \mathrm{TP}/(\mathrm{TP}+\mathrm{FN}) \tag{5}$$

$$F = 2 \times P \times R/(P+R) \tag{6}$$

where TP is the true positives, i.e. the number of changed pixels correctly detected; FP is the false positives, i.e. the number of unchanged pixels incorrectly flagged as changed; and FN is the false negative, i.e. the number of changed pixels incorrectly flagged as unchanged (Powers, 2011).

Moreover, the McNermar's test (Agresti, 2019) is used to assess the levels of statistical significant difference for the forest change detection accuracy. It is a non-parametric test applied to confusion matrices that have a 2 × 2 dimension, which is based on the standardized normal statistic. The test value Z can be calculated as:

$$Z = \frac{|f_{12} - f_{21}|}{\sqrt{f_{12}+f_{21}}} \tag{7}$$

where f_{12} and f_{21} represent the off-diagonal entries in the matrix. The difference between a pair of classifications was considered statistically significant at a confidence of 95% if the calculated Z is greater than 1.96.

4. Results

4.1. Parameter impacts of DCVA

4.1.1. Impact of global magnitude threshold

The global threshold T is to determine the candidate changed pixels from all pixels, which is automatically determined by EM algorithm. It is necessary to analyze the impact of the threshold T on the change detection results and to reveal whether the automatically determined magnitude threshold have a significant impact on the accuracy of the change detection. Fig. 4 shows the accuracy variation of the final change detection results with different global magnitude thresholds.

Obviously, different datasets have dissimilar global magnitude thresholds, but there is a threshold range that the change of accuracy is minimal for every change type. A small global magnitude threshold may result in that the angle clustering is affected by too many false changed pixels, and a large threshold may lead to the absence of many changed pixels in the clustering set. Both above cases can result in failure to determine the direction range of the changed pixels, such as the change of direction range in (b), (c), (e), and (f). Usually, the change of direction range leads to the change of accuracy. The k-means clustering can produce reliable direction range only when the global magnitude threshold is in a certain threshold range, in which the effects of unchanged pixels are effectively eliminated and more changed pixels are hold in the clustering set. The threshold automatically obtained by EM algorithm is in this threshold range as shown in Fig. 4, demonstrating the effectiveness of the adopted EM method for determining the global threshold T.

4.1.2. Impact of number of clusters

The k-means algorithm is used to partition θ of the candidate changed pixels into several direction ranges. The number of clusters should be close to the number of change types. If k is far smaller than the number of change types, the different change types cannot be distinguished. On the contrary, if k is far larger than the number of change types, the changed pixels of a change type may be separated into small subgroups and too many local thresholds need to be set. Therefore, it is necessary to analyze the impact of the number of clusters to the accuracy of change detection results, as shown in Fig. 5, which gives a hint to find the optimal number of clusters.

Fig. 5 shows that a too small k value would do harm to the change detection accuracy, but an exceptionally large k value would not lower the accuracy in most cases. The number of forest change types in dataset 1–3 is 1, 2, and 3, respectively, while the optimal k for the three datasets

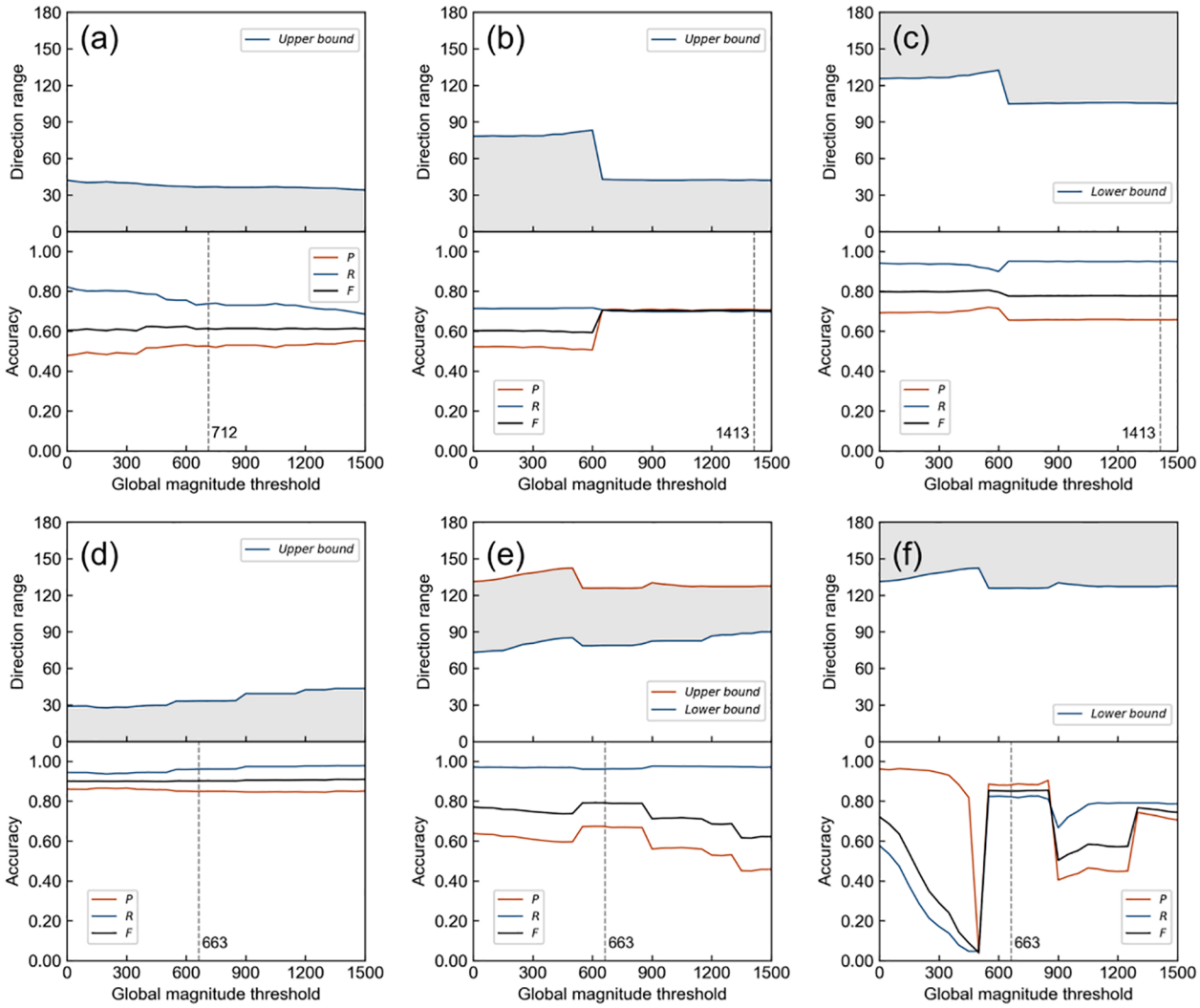

Fig. 4. Impact of the global magnitude threshold to the accuracy of change detection results. (a) dataset 1, A to BC; (b) dataset 2, A to BC; (c) dataset 2, BC to W; (d) dataset 3, A to C; (e) dataset 3, A to CB; and (f) dataset 3, A to S. The gray area between the upper bound and the lower bound indicates the direction range for the corresponding change type. The vertical black dotted line represents the automatically determined global threshold, which located in the threshold range with high accuracy.

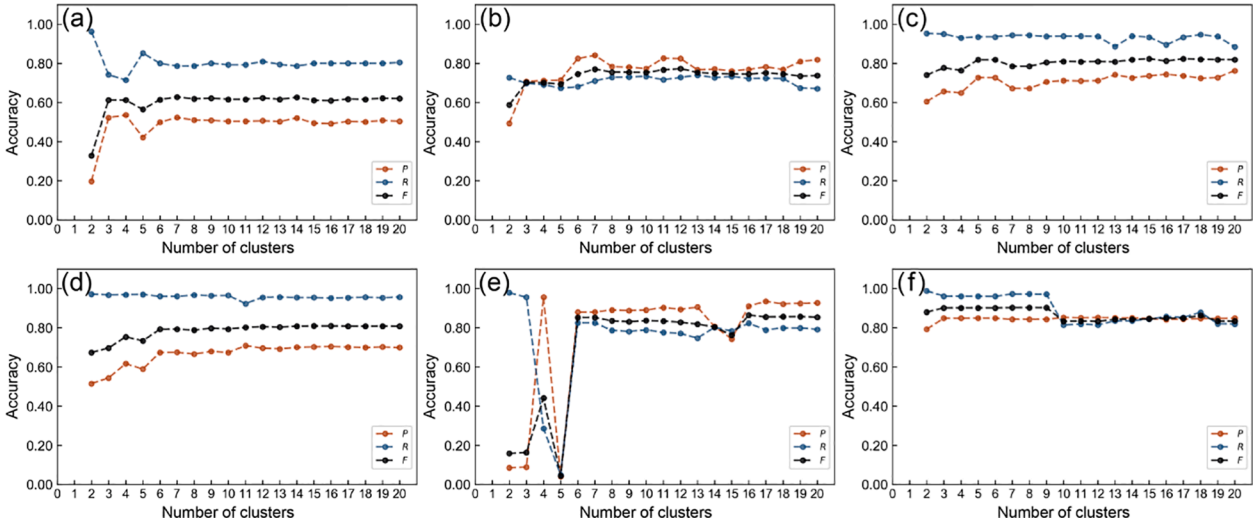

Fig. 5. Impact of the number of clusters *k* to the accuracy of change detection results. (a) dataset 1, A to BC; (b) dataset 2, A to BC; (c) dataset 2, BC to W; (d) dataset 3, A to C; (e) dataset 3, A to CB; and (f) dataset 3, A to S.

are all greater than the number of change types. This is because there are other change types and false changes in the candidate changed pixels for clustering. On the contrary, a too large k produces too many clusters. The change magnitude of each cluster can be rightly segmented in the successive local thresholding procedure, so that the change detection accuracy keeps almost flat. However, this would increase the labor for determining the local thresholds. Thus, the smallest k value that can achieve high change detection accuracy is viewed as optimal and preferred. Accordingly, the optimal k value for dataset 1–3 is 3, 6, and 6, respectively.

From the above analysis, the optimal k would vary for different datasets. Is there an effective method to automatically determine a suitable k for each dataset? For k-means clustering, there are several commonly used methods to automatically determine the optimal k, such as gap statistic (Tibshirani et al., 2001), elbow method (Thorndike, 1953), and silhouette coefficient (Rousseeuw, 1987). The results of the three methods are shown in Fig. 6. For gap statistic method, when the number of clusters is k, $G(k)$ can be regarded as the difference between the loss of random samples and the loss of actual samples, and S_k is the simulation error calculated from the standard deviation of B Monte Carlo replicates. When $G(k) - (G(k+1) - S_{k+1})$ changes from negative to positive for the first time, the corresponding k is viewed as optimal. In Fig. 6 (a)–(c), although the number of change types is different, the automatically obtained k by this method are all equal to 3. For elbow method, the optimal k is found when the slope of the distortion suddenly changes (usually increases), which is like the "elbow". In Fig. 6 (d), the elbow corresponds to the position where k is equal to 3. But in Fig. 6 (e) and (f), there is no obvious elbow in the curve of distortion. For silhouette coefficient method, when silhouette coefficient is close to 1, the clustering result is more reasonable. Since the optimal k is generally not equal to 2, the case where k is equal to 2 is excluded for consideration. In Fig. 6 (g)–(i), the maximum silhouette coefficients all correspond to the position where k is equal to 3. But in Fig. 6 (i), the silhouette coefficient suddenly increases when k is equal to 6, which is similar to the change in Fig. 5 (e). In summary, it is difficult to determine the optimal number of clusters with these automatic methods when extracting changed pixels and their change types from remotely sensed images. The silhouette coefficient method may be the most promising method to determining the optimal k in forest change detection.

4.1.3. Impact of local magnitude threshold

The final changed pixels for each change type are determined by setting different local thresholds for each direction range. Therefore, it is necessary to analyze the impact of the local magnitude thresholds on the accuracy of change detection results. The accuracy curves of the three datasets are shown in Fig. 7, in which the local magnitude thresholds automatically determined by EM algorithm are flagged as vertical black dotted lines. The comparison of the change detection results based on the automatic local magnitude threshold and the optimal local magnitude threshold is shown in Fig. 8.

As shown in Fig. 7, the accuracy corresponding to all change types satisfies the trend of first increasing and then decreasing as the local threshold increases. But for different change types, there are differences in the shape of the accuracy curve. The optimal local magnitude threshold is closely related to the change type, which is different for different change types. In Fig. 7 (a) and (b), because the change types are both A to BC, the optimal local threshold is similar, which is 1022 and 1192, respectively. In Fig. 7 (c)–(f), which respectively correspond to BC to W, A to C, A to CB, and A to S, the optimal local threshold is different, which is 1769, 1694, 899, and 1224, respectively. Moreover, the change types related to cloud, like A to C and A to S, are relatively insensitive to the change of local threshold, which are shown in Fig. 7 (d) and (f). The above results further demonstrate the necessity of determining different local thresholds for different forest change types.

Also as shown in Fig. 7, the automatic local magnitude thresholds are usually smaller than the optimal local magnitude thresholds, which results in lower P value and thus lower F value. However, as compared in Fig. 8, the general pattern of the results between the automatic

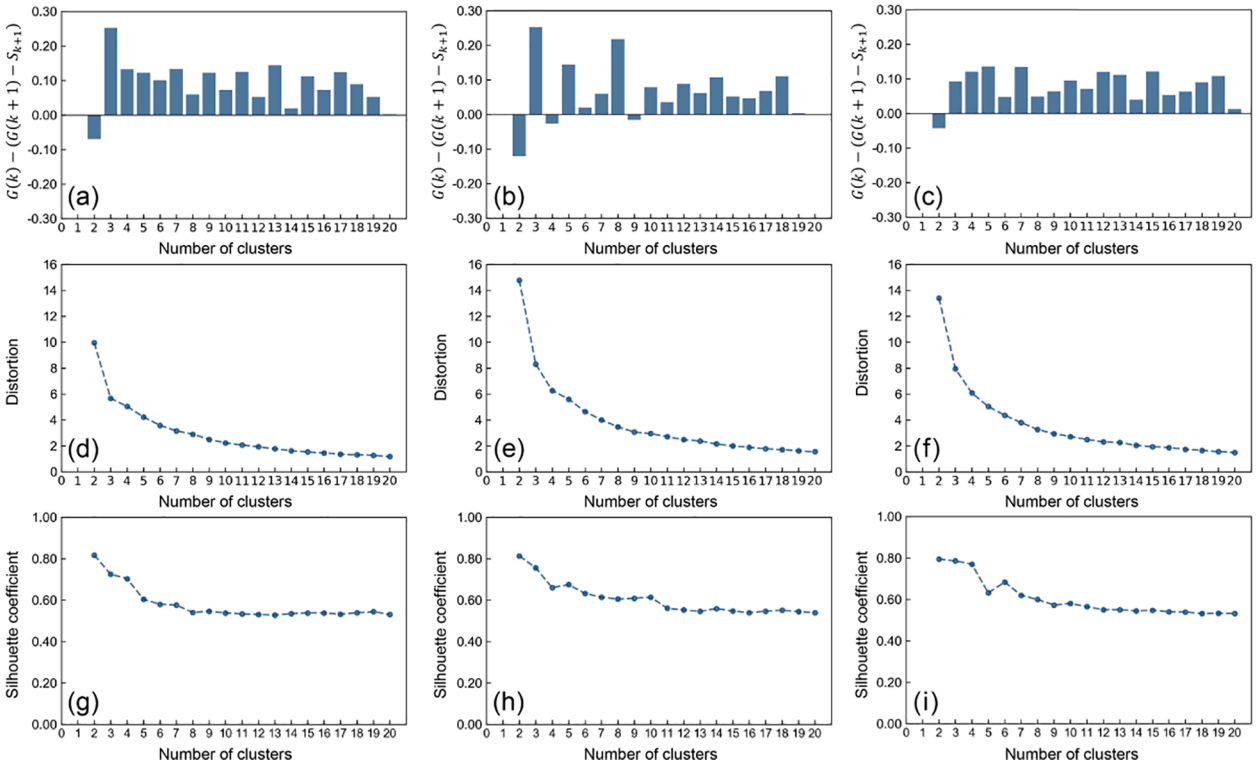

Fig. 6. Results of the gap statistic, elbow method, and silhouette coefficient used to determine the optimal k for k-means clustering. (a)–(c) are gap statistic of dataset 1, 2, and 3, respectively; (d)–(f) are distortion of elbow method of dataset 1, 2, and 3, respectively; and (g)–(i) are silhouette coefficient of dataset 1, 2, and 3, respectively.

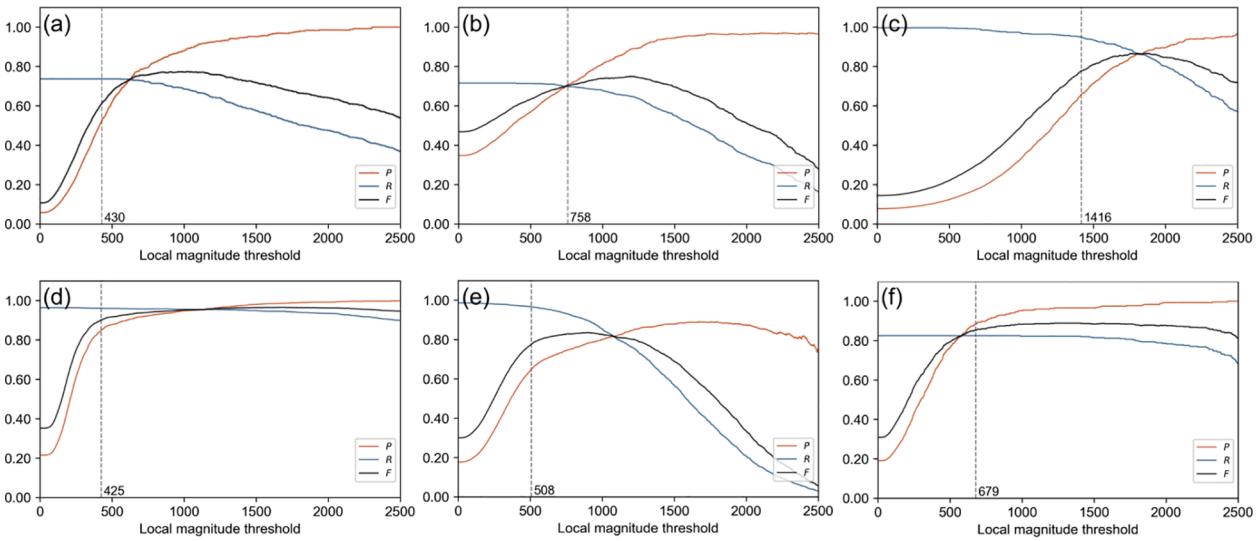

Fig. 7. Impact of the local magnitude threshold to the accuracy of change detection results. (a) dataset 1, A to BC; (b) dataset 2, A to BC; (c) dataset 2, BC to W; (d) dataset 3, A to C; (e) dataset 3, A to CB; and (f) dataset 3, A to S. The vertical black dotted line represents the automatically determined local thresholds.

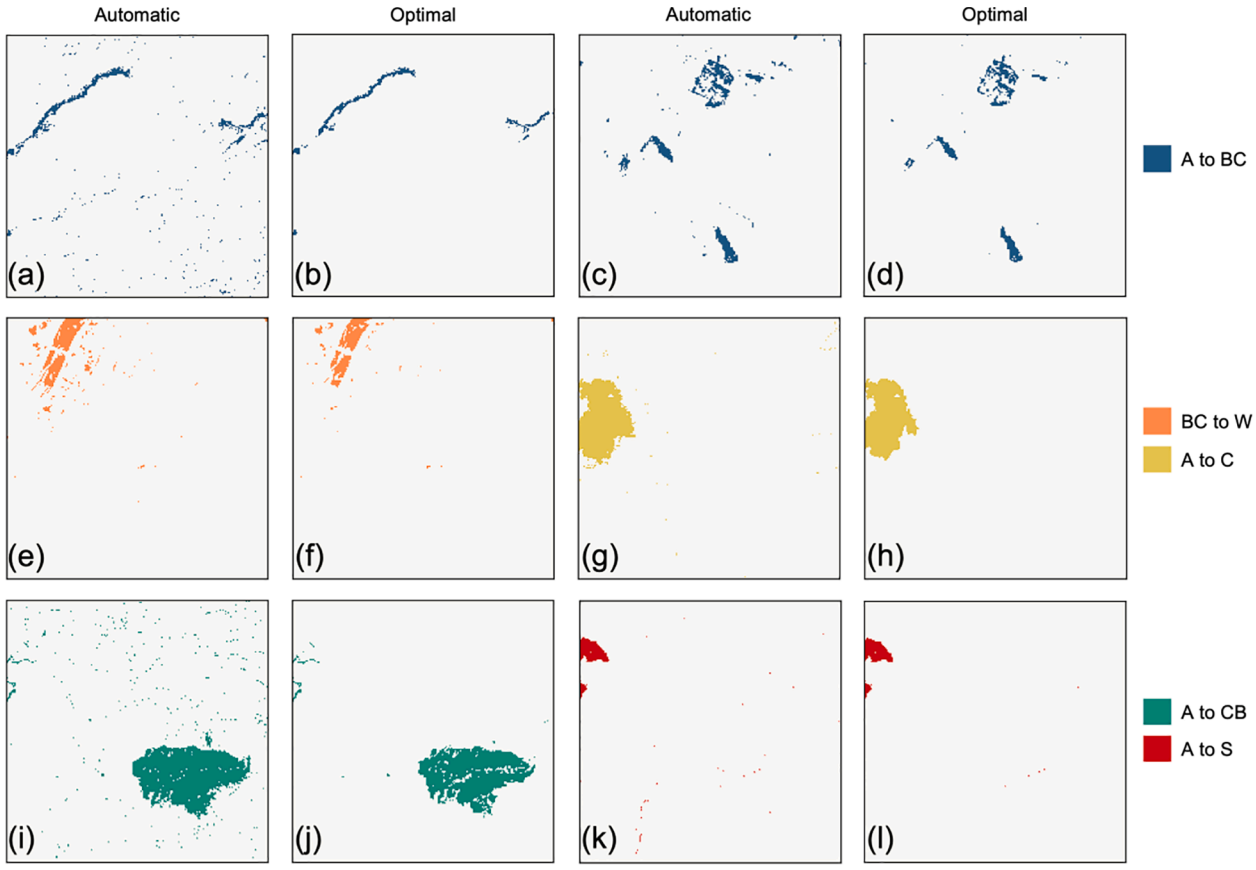

Fig. 8. Comparison of the forest change detection results based on the automatic and the optimal local magnitude threshold. (a) dataset 1, A to BC, automatic; (b) dataset 1, A to BC, optimal; (c) dataset 2, A to BC, automatic; (d) dataset 2, A to BC, optimal; (e) dataset 2, BC to W, automatic; (f) dataset 2, BC to W, optimal; (g) dataset 3, A to C, automatic; (h) dataset 3, A to C, optimal; (i) dataset 3, A to CB, automatic; (j) dataset 3, A to CB, optimal; (k) dataset 3, A to S, automatic; and (l) dataset 3, A to S, optimal.

thresholds and the optimal thresholds are similar, the difference mainly comes from the meaningless small changed areas caused by the salt and pepper noise. In this case, we proposed to add a post-processing step on the result produced by the automatic thresholds by removing the meaningless small changed areas, and the result is shown in Fig. 9. After post-processing, the accuracy of the automatic threshold for all change types has been improved, as can be seen from Table 2. Specifically, for A to BC in dataset 1, *F* is increased by 23%, and for A to BC in dataset 2, *F* is increased by 7%. For BC to W, A to C, A to CB, and A to S, *F* is increased by 12%, 2%, 6%, and 5%, respectively. In addition, the accuracy of the

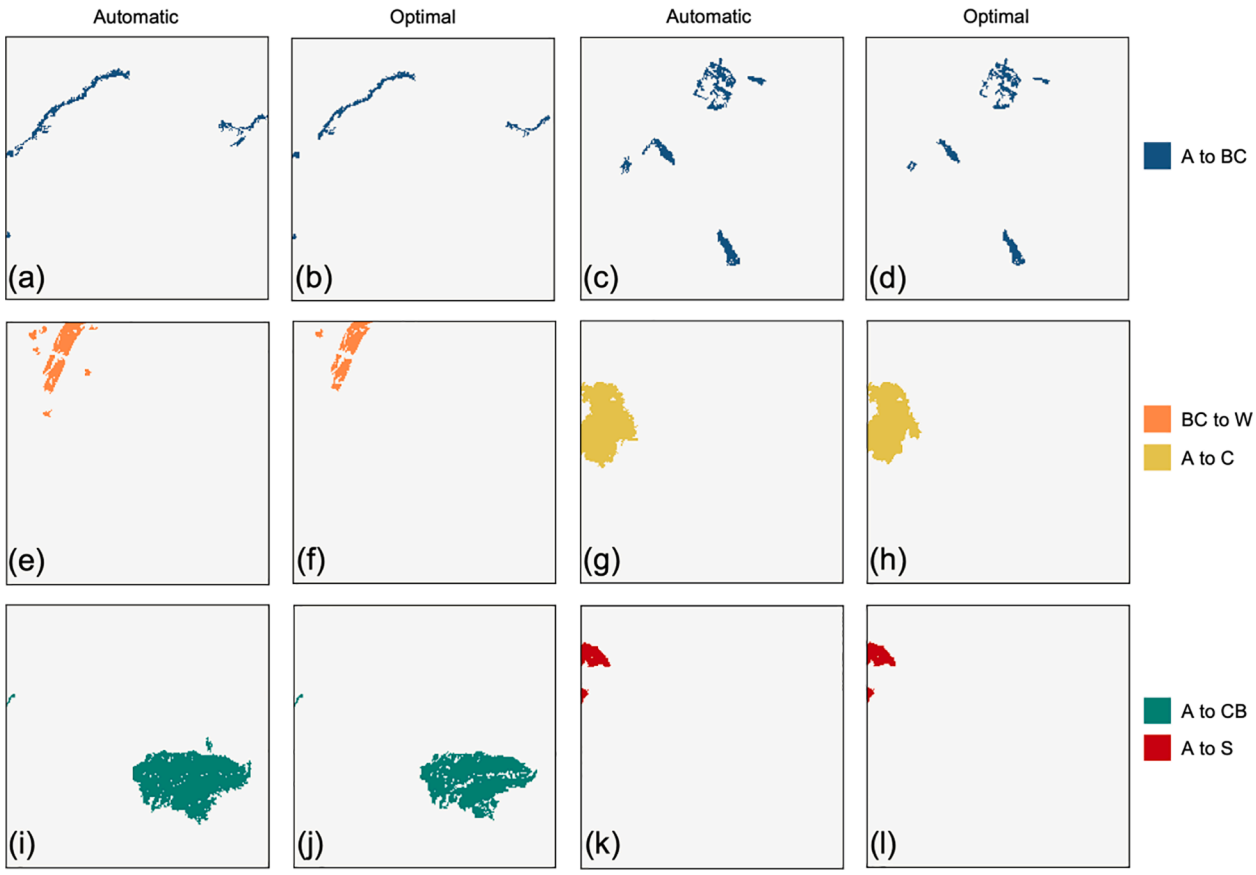

Fig. 9. Comparison of the post-processing results based on the automatic and the optimal local magnitude threshold. (a) dataset 1, A to BC, automatic; (b) dataset 1, A to BC, optimal; (c) dataset 2, A to BC, automatic; (d) dataset 2, A to BC, optimal; (e) dataset 2, BC to W, automatic; (f) dataset 2, BC to W, optimal; (g) dataset 3, A to C, automatic; (h) dataset 3, A to C, optimal; (i) dataset 3, A to CB, automatic; (j) dataset 3, A to CB, optimal; (k) dataset 3, A to S, automatic; and (l) dataset 3, A to S, optimal.

Table 2
Accuracy comparison of the forest change detection results before and after post-processing.

Dataset		1		2				3					
Change type		A to BC		A to BC		BC to W		A to C		A to CB		A to S	
Before	T	automatic	optimal	automatic	optimal	automatic	optimal	automatic	optimal	automatic	optimal	automatic	optimal
	P	0.53	0.89	0.71	0.89	0.66	0.85	0.85	0.99	0.65	0.78	0.88	0.97
	R	0.74	0.68	0.70	0.65	0.95	0.88	0.96	0.95	0.97	0.90	0.83	0.82
	F	0.61	0.77	0.70	0.75	0.78	0.87	0.90	0.97	0.78	0.84	0.85	0.89
After	T	automatic	optimal	automatic	optimal	automatic	optimal	automatic	optimal	automatic	optimal	automatic	optimal
	P	0.75	0.91	0.82	0.93	0.81	0.94	0.88	0.99	0.72	0.80	0.97	0.98
	R	0.74	0.67	0.69	0.64	0.95	0.85	0.96	0.95	0.97	0.90	0.82	0.82
	F	0.75	0.77	0.75	0.75	0.87	0.89	0.92	0.97	0.83	0.84	0.89	0.89

Note: T refers to local magnitude threshold.

optimal threshold has also improved slightly. In summary, the accuracy of the automatic thresholds is similar with that of the optimal thresholds, and the difference of accuracy between them is mainly caused by some scattered pixels in the result of the automatic thresholds.

4.1.4. Summary of parameter impacts

The key parameters of each step of DCVA have been carefully analyzed. The first step is to determine the candidate changed pixels from all pixels by a global threshold *T*. The second step is to determine the change types based on the directions of the candidate changed pixels. Finally, the changed pixels for each change type are determined for each direction range. The global magnitude threshold affects the directions of the candidate changed pixels, and the EM method is validated to be effective to determine the global magnitude threshold. The number of clusters *k* determines the effectiveness of direction ranges and thus influences the final change detection results. A too small *k* value is harmful to accuracy and thus not suggested. An exceptionally large *k* value would not do harm to accuracy but increase the labor of determining local thresholds in the last step. A relatively large *k* value is preferred, and how to automatically determine a suitable *k* value remains dissolved. At last, the local magnitude threshold directly affects the accuracy of the final change detection results, where the automatically determined local thresholds are validated to be effective combined with the post-processing by removing meaningless small changed areas.

4.2. Comparison between CVA and DCVA

The performance of CVA and DCVA is compared. CVA is a common

method of change detection. The magnitude of CV is first used to detect change area, followed by detecting change type with the direction of CV. By contrary, in DCVA, the change type is first determined, followed by detecting change area for each change type, with the aim of eliminating false changes by clarifying the magnitude threshold in each direction range. In order to fairly compare the performance of CVA and DCVA, the direction range of CVA was set as same as that in DCVA, and the magnitude threshold of CVA was set optimal, which was determined by the accuracy curve of the global magnitude threshold.

The results obtained by CVA and DCVA are shown in Fig. 10. For dataset 1, CVA and DCVA results are similar, where the main forest change area is detected, but it can be found that the changed area by CVA in the black dotted circle is thinner than that by DCVA, which means that the forest changed pixels located at the boundary of the forest changed area cannot be detected by CVA. For dataset 2, compared with CVA, DCVA can detect the real forest changed pixels in the yellow dotted circle while effectively removing the false changes in the black dotted circle, and the result is more similar to the reference in the red dotted circle with complex spectral information. For dataset 3, in the black dotted circle, the results obtained by CVA and DCVA are comparable with the real forest changed pixels. In the middle part of the black dotted circle, DCVA and CVA both determine the unchanged pixels as the forest changed pixels, and in the lower part of the black dotted circle, some forest changed pixels were not detected. In the red dotted circle, DCVA obtains a more accurate forest change area than CVA. In summary, the change detection results obtained by CVA may miss some change areas, and DCVA presents advantages by setting different magnitude thresholds in different direction ranges.

The change detection accuracies of CVA and DCVA are shown in Table 3. Comparing with CVA, DCVA has an improvement in the

Table 3
Accuracy comparison and statistical significance of the difference between the forest change detection results produced by CVA and DCVA.

Dataset		1	2		3		
Change type		A to BC	A to BC	BC to W	A to C	A to CB	A to S
CVA	*P*	0.97	0.96	0.80	0.96	0.84	0.96
	R	0.55	0.50	0.91	0.95	0.78	0.82
	F	0.70	0.65	0.85	0.96	0.81	0.89
DCVA	*P*	0.91	0.93	0.94	0.99	0.80	0.98
	R	0.67	0.64	0.85	0.95	0.90	0.82
	F	0.77	0.75	0.89	0.97	0.84	0.89
CVA vs. DCVA		4.20*	8.29*	5.65*	4.09*	4.13*	2.12*

Note: * indicates significant difference.

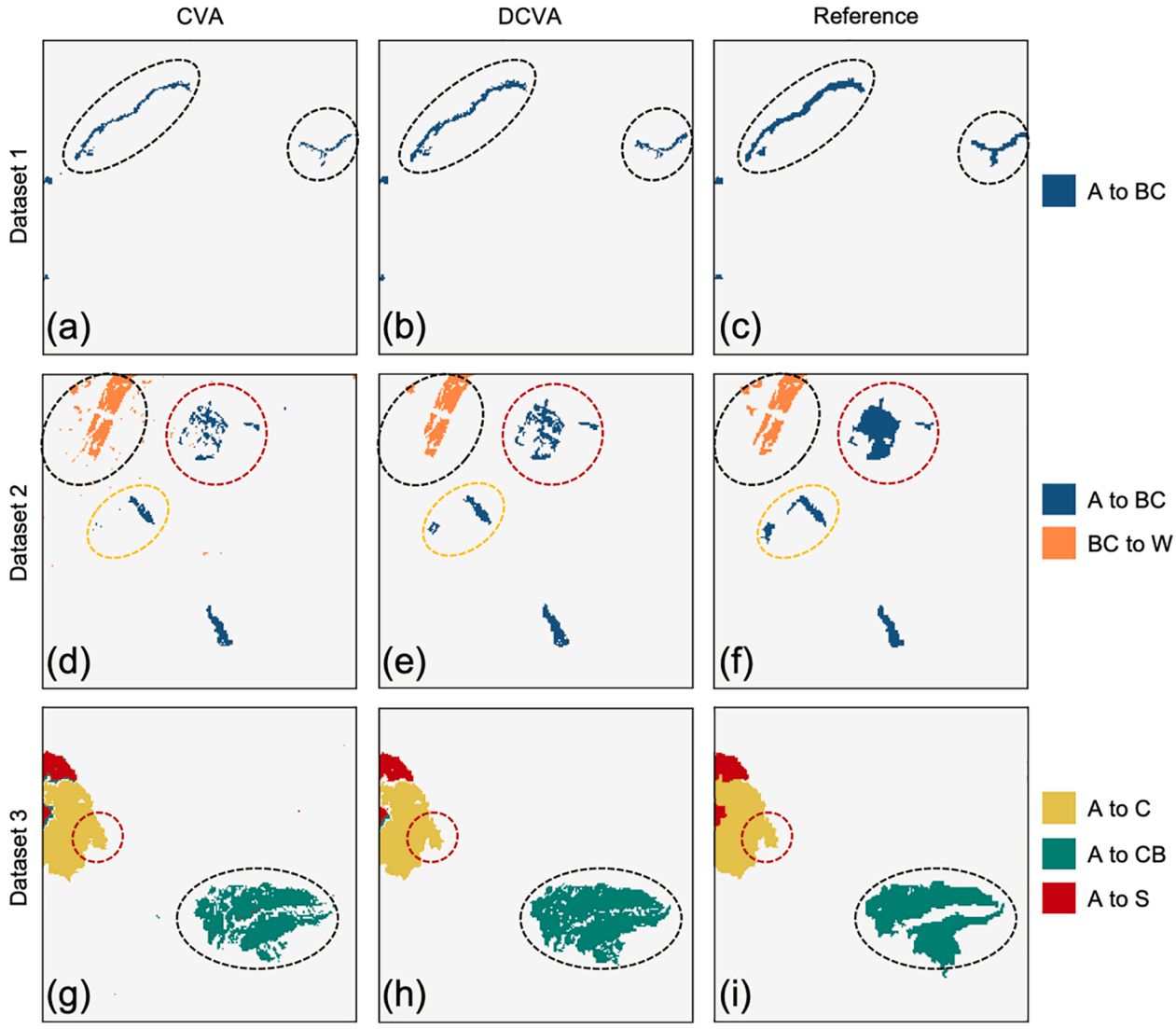

Fig. 10. Comparison of the forest change detection results obtained by CVA and DCVA. (a)–(c) are CVA, DCVA, and reference of dataset 1; (d)–(f) are CVA, DCVA, and reference of dataset 2; and (g)–(i) are CVA, DCVA, and reference of dataset 3.

accuracy. Let F corresponding to DCVA be F_D, F corresponding to CVA be F_C. For dataset 1, the change type is A to BC, and F_D is 10% higher than F_C. For dataset 2, the change types are A to BC and BC to W. For A to BC, F_D is 15% higher than F_C, and for BC to W, F_D is 5% higher than F_C. For dataset 3, the change types are A to C, A to CB, and A to S. For A to C and A to S, F_D is similar with F_C, and for A to CB, F_D is 4% higher than F_C. In summary, For A to BC, the accuracy of DCVA is apparently better than that of CVA. For BC to W and A to CB, the accuracies of DCVA are slightly better than those of CVA. Besides, for A to C and A to S, DCVA and CVA have almost the same accuracies because of the apparent differences between the two images. The differences between CVA and DCVA for all the change types and datasets are statistically significant as shown in Table 3.

The running time of CVA and DCVA is also compared based on the optimal magnitude thresholds and direction ranges. The processing of forest change detection was based on a computer with Intel core i9-10900 (2.8 GHz), RAM of 64 GB, hard disk of 500 GB, and graphics card of NVIDIA GeForce RTX 2060. The operating system is Window 10, and the development environment is Python IDLE. In order to avoid the random error of computing, the running time of the experiment is averaged ten times.

Overall, the running time of the CVA and DCVA are similar for all datasets, as shown in Table 4. For dataset 2 and dataset 3, the running time of DCVA is slightly superior to CVA. Moreover, detecting the change types A to BC and BC to W of dataset 2 takes the longest time when compared to the change types of dataset 1 and dataset 3.

5. Discussion

5.1. Relationship between direction range and change type

For both CVA and DCVA, the change type is determined by the CVs' direction range. Thus, exploring the relation between direction range and change type is important and inevitable. Several studies have illustrated this relation in two ways. The first way is to associate the direction ranges to different change types extracted from a two- or multi-dimensional space, where the number of change types is usually obtained by a priori knowledge (Bovolo and Bruzzone, 2007; Malila, 1980; Solano-Correa et al., 2019). The other way is to establish a lookup table of change types according to the difference of CVs between any two types of land cover in the samples or classification result (Allen, 2000; Chen et al., 2003; Cohen and Fiorella, 1998). Although these studies have expressed the relation between direction range and change type, due to the influence of the location of study area, phenology, and participating features (e.g. spectral bands, TC indices, vegetation indices), there is no universal quantitative relation between them.

For the forest changes in this study, the involved change types are caused by deforestation, degradation, and image conditions (mainly cloud and cloud shadow), thus the first way is chosen to describe the relationship between direction range and change type. In a polar coordinate space, each change type corresponds to a direction range. These direction ranges may be far apart without overlap at all, thus their corresponding change types can be distinguished easily, such as A to BC and BC to W. However, when the direction ranges are very close or even overlapping with each other, the change types will be difficult to be distinguished, such as A to BC and A to S. The key to deal with this situation is to divide into more direction ranges by setting a relatively large k value, and then to merge the direction ranges with the same change type after determining the local threshold for each direction range.

Table 4
Comparison of the running time (millisecond) of CVA and DCVA for forest change detection.

Dataset	1	2	3
CVA	469	496	489
DCVA	469	495	486

5.2. Direction-dominated versus magnitude-dominated

DCVA is "direction-dominated", while CVA is "magnitude-dominated". The comparative analysis in Table 3 is used to show the theoretical upper limit of CVA and DCVA. Specifically, comparing with CVA, DCVA has a certain improvement in accuracy for A to BC, A to CB, and BC to W. Nevertheless, when dealing with cloud-related changes, like A to S and A to C, the two strategies perform very closely.

CVA is "magnitude-dominated" by setting only one global magnitude threshold at first for different change types, while DCVA is "direction-dominated" by determining change types according to change direction at first, followed by setting different magnitude threshold for each change type. For CVA, the global magnitude threshold would underestimate or over-estimate changed pixels, and thus the accuracy will be significantly reduced. For DCVA, the use of direction range can effectively distinguish change types, and the local magnitude threshold in each direction range makes it possible to obtain a more accurate change area. Comparing with CVA, DCVA holds the advantage of accurately detecting change areas for different change types by considering the specific characteristic for each change type.

Certainly, when using DCVA for change detection, "direction-dominated" also has its shortage. If there are no real changed pixels in a direction range, but the candidate changed pixels cover this direction range, then the obtained change detection result will inevitably include pseudo-changed pixels in this direction range after setting local thresholds. In this case, it is found that the changed pixels in some direction range are randomly and uniformly distributed in the image, which should be judged as pseudo-changed pixels and be removed from the change detection result.

6. Conclusion

A semi-automatic DCVA method was proposed for detecting forest changes in this study. It is composed of three steps: determining candidate changed pixels, determining direction ranges for different forest change types, and determining final changed pixels for each forest change type. Validated by experiments on Sentinel-2A images, DCVA can achieve high accuracies in terms of both change area and change type by clarifying the magnitude threshold in each direction range.

By analyzing parameter impacts of DCVA and comparing the performance of DCVA and CVA, we found that: The global magnitude threshold affects the directions of the candidate changed pixels, the number of clusters determines the effectiveness of direction ranges, and the local magnitude threshold directly affects the accuracy of the final change detection result; and CVA is "magnitude-dominated" by setting only one magnitude threshold for different change types, while DCVA is "direction-dominated" by determining change types according to change direction at first, followed by setting different magnitude threshold for each change type. In this case, DCVA holds the advantage of accurately detecting change areas for different change types by considering the specific characteristic for each change type.

Future developments of this work include: The types of forest changes in the study are limited and are only for the Sentinel-2A image in summer. Later, more spectral samples can be collected from images to expand the seasonal coverage, number of types, etc., and verify its portability and scalability on other remote sensing data; The direction ranges in the study are obtained by k-means clustering, which makes the number of cluster k still need to be manually assigned according to the number of change types. Therefore, the spatial context information of the change direction map can be combined to construct a strategy that can automatically determine the change types and its angle ranges in the future; and For the change magnitude distribution, Zanetti et al. (2015) demonstrated the Rayleigh-Rice model is the one that better fits the

distribution, among other statistical models proposed in literature. We expect to achieve higher accuracy using Rayleigh-Rice distribution than Gaussian-Gaussian distribution in modeling the change magnitude in the EM algorithm in the future.

CRediT authorship contribution statement

Pengfeng Xiao: Investigation, Conceptualization, Methodology, Writing – review & editing, Resources, Funding acquisition, Supervision. **Guangwei Sheng:** Investigation, Methodology, Data curation, Software, Visualization, Writing– original draft. **Xueliang Zhang:** Methodology, Writing – review & editing, Funding acquisition, Supervision. **Hao Liu:** Methodology, Software, Writing – review & editing. **Rui Guo:** Software, Validation.

Declaration of Competing Interest

The authors declare that they have no known competing financial interests or personal relationships that could have appeared to influence the work reported in this paper.

Acknowledgements

This work was supported by the National Science and Technology Major Project of China under Grant 21-Y20A06-9001-17/18 and the National Natural Science Foundation of China under Grant 41871235 and Grant 42071297.

References

Agresti, A., 2019. An Introduction to Categorical Data Analysis, third ed. John Wiley & Sons, Hoboken, NJ.

Allen, H., Simonson, W., Parham, E., Santos, E.D.B.E., Hotham, P., 2018. Satellite remote sensing of land cover change in a mixed agro-silvo-pastoral landscape in the Alentejo, Portugal. Int. J. Remote Sens. 39, 4663–4683. https://doi.org/10.1080/01431161.2018.1440095.

Allen, T., 2000. Application of spherical statistics to change vector analysis of Landsat data: southern Appalachian spruce–fir forests. Remote Sens. Environ. 74, 482–493. https://doi.org/10.1016/S0034-4257(00)00140-1.

Bayarjargal, Y., Karnieli, A., Bayasgalan, M., Khudulmur, S., Gandush, C., Tucker, C.J., 2006. A comparative study of NOAA–AVHRR derived drought indices using change vector analysis. Remote Sens. Environ. 105, 9–22. https://doi.org/10.1016/j.rse.2006.06.003.

Bovolo, F., Bruzzone, L., 2011. An adaptive thresholding approach to multiple-change detection in multispectral images. In: 2011 IEEE International Geoscience and Remote Sensing Symposium, Vancouver, BC, Canada, pp. 233–236. https://doi.org/10.1109/IGARSS.2011.6048935.

Bovolo, F., Bruzzone, L., 2007. A theoretical framework for unsupervised change detection based on change vector analysis in the polar domain. IEEE Trans. Geosci. Remote Sens. 45, 218–236. https://doi.org/10.1109/TGRS.2006.885408.

Bovolo, F., Marchesi, S., Bruzzone, L., 2012. A framework for automatic and unsupervised detection of multiple changes in multitemporal images. IEEE Trans. Geosci. Remote Sens. 50, 2196–2212. https://doi.org/10.1109/TGRS.2011.2171493.

Byrne, G.F., Crapper, P.F., Mayo, K.K., 1980. Monitoring land-cover change by principal component analysis of multitemporal landsat data. Remote Sens. Environ. 10, 175–184. https://doi.org/10.1016/0034-4257(80)90021-8.

Chazdon, R.L., Brancalion, P.H.S., Laestadius, L., Bennett-Curry, A., Buckingham, K., Kumar, C., Moll-Rocek, J., Vieira, I.C.G., Wilson, S.J., 2016. When is a forest a forest? Forest concepts and definitions in the era of forest and landscape restoration. Ambio 45, 538–550. https://doi.org/10.1007/s13280-016-0772-y.

Chen, J., Gong, P., He, C., Pu, R., Shi, P., 2003. Land-use/land-cover change detection using improved change-vector analysis. Photogramm. Eng. Remote Sens. 69, 369–379. https://doi.org/10.14358/PERS.69.4.369.

Chen, Q., Chen, Y., 2016. Multi-feature object-based change detection using self-adaptive weight change vector analysis. Remote Sens. 8, 549. https://doi.org/10.3390/rs8070549.

Chen, X., Chen, J., Shi, Y., Yamaguchi, Y., 2012. An automated approach for updating land cover maps based on integrated change detection and classification methods. ISPRS J. Photogramm. Remote Sens. 71, 86–95. https://doi.org/10.1016/j.isprsjprs.2012.05.006.

Cohen, W.B., Fiorella, M.L., 1998. Comparison of methods for detecting conifer forest change with thematic mapper imagery. In: Lunetta, R.S., Elvidge, C.D. (Eds.), Remote Sensing Change Detection: Environmental Monitoring Methods and Applications. Ann Arbor Press, Chelsea, MI, pp. 89–102.

Cohen, W.B., Yang, Z., Healey, S.P., Kennedy, R.E., Gorelick, N., 2018. A LandTrendr multispectral ensemble for forest disturbance detection. Remote Sens. Environ. 205, 131–140. https://doi.org/10.1016/j.rse.2017.11.015.

Collins, J.B., Woodcock, C.E., 1996. An assessment of several linear change detection techniques for mapping forest mortality using multitemporal landsat TM data. Remote Sens. Environ. 56, 66–77. https://doi.org/10.1016/0034-4257(95)00233-2.

Duveiller, G., Defourny, P., Desclée, B., Mayaux, P., 2008. Deforestation in Central Africa: Estimates at regional, national and landscape levels by advanced processing of systematically-distributed Landsat extracts. Remote Sens. Environ. 112, 1969–1981. https://doi.org/10.1016/j.rse.2007.07.026.

Fernández-Manso, A., Fernández-Manso, O., Quintano, C., 2016. SENTINEL-2A red-edge spectral indices suitability for discriminating burn severity. Int. J. Appl. Earth Obs. Geoinformation 50, 170–175. https://doi.org/10.1016/j.jag.2016.03.005.

Healey, S.P., Cohen, W.B., Yang, Z., Kenneth Brewer, C., Brooks, E.B., Gorelick, N., Hernandez, A.J., Huang, C., Joseph Hughes, M., Kennedy, R.E., Loveland, T.R., Moisen, G.G., Schroeder, T.A., Stehman, S.V., Vogelmann, J.E., Woodcock, C.E., Yang, L., Zhu, Z., 2018. Mapping forest change using stacked generalization: An ensemble approach. Remote Sens. Environ. 204, 717–728. https://doi.org/10.1016/j.rse.2017.09.029.

Hussain, M., Chen, D., Cheng, A., Wei, H., Stanley, D., 2013. Change detection from remotely sensed images: From pixel-based to object-based approaches. ISPRS J. Photogramm. Remote Sens. 80, 91–106. https://doi.org/10.1016/j.isprsjprs.2013.03.006.

Johnson, R.D., Kasischke, E.S., 1998. Change vector analysis: A technique for the multispectral monitoring of land cover and condition. Int. J. Remote Sens. 19, 411–426. https://doi.org/10.1080/014311698216062.

Leichtle, T., Geiß, C., Wurm, M., Lakes, T., Taubenböck, H., 2017. Unsupervised change detection in VHR remote sensing imagery – an object-based clustering approach in a dynamic urban environment. Int. J. Appl. Earth Obs. Geoinformation 54, 15–27. https://doi.org/10.1016/j.jag.2016.08.010.

Liu, B., Chen, Jun, Chen, Jiage, Zhang, W., 2018. Land cover change detection using multiple shape parameters of spectral and NDVI curves. Remote Sens. 10, 1251. https://doi.org/10.3390/rs10081251.

Lu, D., Mausel, P., Brondízio, E., Moran, E., 2004. Change detection techniques. Int. J. Remote Sens. 25, 2365–2401. https://doi.org/10.1080/0143116031000139863.

Lunetta, R.S., Knight, J.F., Ediriwickrema, J., Lyon, J.G., Worthy, L.D., 2006. Land-cover change detection using multi-temporal MODIS NDVI data. Remote Sens. Environ. 105, 142–154. https://doi.org/10.1016/j.rse.2006.06.018.

MacDicken, K.G., 2015. Global forest resources assessment 2015: What, why and how? For. Ecol. Manag. 352, 3–8. https://doi.org/10.1016/j.foreco.2015.02.006.

Malila, W., 1980. Change vector analysis: An approach for detecting forest changes with Landsat. LARS Symp. 326–335.

Marinelli, D., Coops, N.C., Bolton, D.K., Bruzzone, L., 2020. Forest change detection in lidar data based on polar change vector analysis. IEEE Geosci. Remote. Sens. Lett. 1–5 https://doi.org/10.1109/LGRS.2020.3022282.

Moon, T.K., 1996. The expectation-maximization algorithm. IEEE Signal Process. Mag. 13, 47–60. https://doi.org/10.1109/79.543975.

Muchoney, D.M., Haack, B.N., 1994. Change detection for monitoring forest defoliation. Photogramm. Eng. Remote Sens. 60, 1243–1252.

Nackaerts, K., Vaesen, K., Muys, B., Coppin, P., 2005. Comparative performance of a modified change vector analysis in forest change detection. Int. J. Remote Sens. 26, 839–852. https://doi.org/10.1080/0143116032000160462.

Oliveira, E.R., Disperati, L., Cenci, L., Gomes Pereira, L., Alves, F.L., 2019. Multi-Index Image Differencing Method (MINDED) for flood extent estimations. Remote Sens. 11, 1305. https://doi.org/10.3390/rs11111305.

Powers, D., 2011. Evaluation: From precision, recall and F-factor to ROC, informedness, markedness & correlation. J. Mach. Learn. Technol. 2, 37–63.

Rokni, K., Ahmad, A., Solaimani, K., Hazini, S., 2015. A new approach for surface water change detection: Integration of pixel level image fusion and image classification techniques. Int. J. Appl. Earth Obs. Geoinformation 34, 226–234. https://doi.org/10.1016/j.jag.2014.08.014.

Rousseeuw, P.J., 1987. Silhouettes: A graphical aid to the interpretation and validation of cluster analysis. J. Comput. Appl. Math. 20, 53–65. https://doi.org/10.1016/0377-0427(87)90125-7.

Singh, A., 1989. Digital change detection techniques using remotely-sensed data. Int. J. Remote Sens. 10, 989–1003. https://doi.org/10.1080/01431168908903939.

Solano-Correa, Y.T., Bovolo, F., Bruzzone, L., 2019. An approach to multiple change detection in VHR optical images based on iterative clustering and adaptive thresholding. IEEE Geosci. Remote Sens. Lett. 1–5 https://doi.org/10.1109/LGRS.2019.2896385.

Solano-Correa, Y.T., Bovolo, F., Bruzzone, L., Fernandez-Prieto, D., 2017. Spatio-temporal evolution of crop fields in Sentinel-2 satellite image time series. In: 2017 9th International Workshop on the Analysis of Multitemporal Remote Sensing Images (MultiTemp), pp. 1–4. https://doi.org/10.1109/Multi-Temp.2017.8035236.

Sun, H., Zhou, W., Zhang, Y., Cai, C., Chen, Q., 2019. Integrating spectral and textural attributes to measure magnitude in object-based change vector analysis. Int. J. Remote Sens. 40, 5749–5767. https://doi.org/10.1080/01431161.2019.1582111.

Tewkesbury, A.P., Comber, A.J., Tate, N.J., Lamb, A., Fisher, P.F., 2015. A critical synthesis of remotely sensed optical image change detection techniques. Remote Sens. Environ. 160, 1–14. https://doi.org/10.1016/j.rse.2015.01.006.

Thorndike, R.L., 1953. Who belongs in the family? Psychometrika 18, 267–276. https://doi.org/10.1007/BF02289263.

Tibshirani, R., Walther, G., Hastie, T., 2001. Estimating the number of clusters in a data set via the gap statistic. J. R. Stat. Soc. Series B Stat. Methodol. 63, 411–423. https://doi.org/10.1111/1467-9868.00293.

Trumbore, S., Brando, P., Hartmann, H., 2015. Forest health and global change. Science 349, 814–818. https://doi.org/10.1126/science.aac6759.

Vogelmann, J.E., Gallant, A.L., Shi, H., Zhu, Z., 2016. Perspectives on monitoring gradual change across the continuity of Landsat sensors using time-series data. Remote Sens. Environ., Landsat 8 Science Results 185, 258–270. https://doi.org/10.1016/j.rse.2016.02.060.

Xian, G., Homer, C., Fry, J., 2009. Updating the 2001 National Land Cover Database land cover classification to 2006 by using Landsat imagery change detection methods. Remote Sens. Environ. 113, 1133–1147. https://doi.org/10.1016/j.rse.2009.02.004.

Zanetti, M., Bovolo, F., Bruzzone, L., 2015. Rayleigh-Rice mixture parameter estimation via EM algorithm for change detection in multispectral images. IEEE Trans. Image Process 24, 5004–5016. https://doi.org/10.1109/TIP.2015.2474710.

Zanotta, D.C., Bruzzone, L., Bovolo, F., 2014. Detection of specific changes in image time series by an adaptive change vector analysis. In: 2014 IEEE Geoscience and Remote Sensing Symposium, Quebec City, QC, Canada, pp. 1285–1288. https://doi.org/10.1109/IGARSS.2014.6946668.

Zhu, Z., 2017. Change detection using Landsat time series: A review of frequencies, preprocessing, algorithms, and applications. ISPRS J. Photogramm. Remote Sens. 130, 370–384. https://doi.org/10.1016/j.isprsjprs.2017.06.013.